doi: 10.1111/j.1460-2695.2007.01158.x

Comparative assessment of fatigue and fracture behaviour of cast and forged railway wheels

S. TARAFDER[1], S. SIVAPRASAD[1] and V. R. RANGANATH[2]

[1]*National Metallurgical Laboratory, Jamshedpur 831007, India*, [2]*National Aerospace Laboratories, Bangalore 560017, India*

Received in final form 16 May 2007

ABSTRACT A comparative evaluation of fatigue and fracture behaviour of commercially produced cast and forged rail wheels has been made using specimens extracted from various locations of the wheel quadrant. A systematic investigation in the web and rim regions of the wheel quadrant with various notch orientations showed that the forged material exhibited a better intrinsic resistance to fatigue crack growth than the cast material. Since linear elastic fracture mechanics (LEFM) based fracture toughness could not be validated for both the cast and forged wheel material, elastic plastic fracture mechanics (EPFM) based characteristic fracture toughness was used. Results showed that fracture resistance of the forged material is superior to that of the cast material. Cast wheel specimens exhibited unstable crack extension in comparison to substantial stable tearing in forged specimens. Microstructural and fractographic analyses showed that the cast wheel material contained large amounts of inclusions. The poor fracture resistance of cast wheel material is therefore attributed to the inferior material quality.

Keywords cast and forged rail wheels; FCGR; fracture.

NOMENCLATURE

a, a_o, Δa = Instantaneous crack length, original crack length, crack extension
B = Specimen thickness
C = Constant in Paris equation
C_1, C_2 = Coefficients in the $\mathcal{J}$-Δa relation
da/dN = Fatigue crack growth rate
$\mathcal{J}$, $\mathcal{J}$-R, $\mathcal{J}_{1c}$ = An energy based ductile fracture toughness characterizing parameter, $\mathcal{J}$ based fracture resistance curve, ductile fracture toughness
K_{Ic}, K_Q = Plane strain fracture toughness, conditional fracture toughness
m = Exponent in the Paris equation
N = Number of fatigue cycles
P_{max} = Maximum load in load–displacement curve during fracture test
P_Q = Critical load on load–displacement curve at which crack initiation takes place
R = Ratio of minimum stress intensity factor to maximum stress intensity factor
v = Displacement
W = Specimen width

Correspondence: S. Tarafder. E-mail: star@nmlindia.org

ΔK, ΔK_o, ΔK_{eff}, ΔK_{app}, ΔK_{th} = Stress intensity factor range, initial stress intensity factor range, effective stress intensity factor range, applied stress intensity factor range, threshold value of stress intensity factor range
σ_{YS} = Yield stress
σ_Y = Flow stress

INTRODUCTION

Wheels for passenger railway cars are conventionally made by forging. Wheel forging is an established process that, together with development of rim quenching techniques, is able to produce wheel-sets of adequate quality economically. An innovation in the manufacture of railway wheels, primarily for the purpose of freight haulage, is the employment of near-net shape casting technology.[1,2] These are patented processes using chill casting, advanced gating and pressure-pouring techniques. The satisfactory performance of cast wheels, and the favourable economics of their production, has prompted the demand for their usage in passenger traffic also. Since passenger transport entails the adoption of considerably higher levels of safety and minimization of failure risks, it is imperative that forged and cast wheels be critically compared with respect to their properties and performance.

The life of railway wheels is generally measured in terms of tread wear, which is governed by various factors, such as mode of operation, bogie design, axle load, frequency of braking etc. However, railway wheels may fail prematurely, and often with grave consequences, through the process of initiation and growth of fatigue cracks, ultimately leading to catastrophic fracture. The generalised sequence of events that are thought to occur during the process of failure of railway wheels are the following:

1. initiation of cracks at the tread surface or in the interior by fatigue, often through rolling contact fatigue or thermal fatigue mechanisms.
2. growth of microstructurally short fatigue cracks through the hardened surface layers at the tread.
3. growth of 'long' fatigue cracks in the wheel material.
4. stable or catastrophic fracture under operating or accidental loads ensuing from long cracks that have achieved critical size.

Some of the above events are described in depth in the literature.[3,4]

It may be noted that initiation and early growth of tread surface fatigue cracks often takes place through thermal fatigue mechanism when an appreciable thermal load arising from braking and friction is present. At times, cracks may initiate from the interior, often at the junction of the hardened layer and the bulk.

From the point of view of safety, the resistance of the wheel material to fatigue and fracture is thus of paramount importance. A number of reports on thermal fatigue, rolling contact fatigue and fracture behaviour of railway wheels are available in the literature.[5–14] Most of these investigations report the assessment of integrity of forged wheel materials except for reference 14, where the fracture behaviour of railway wheels made of austempered ductile iron (ADI) with graphite nodules has been discussed. A systematic comparison of wheel materials manufactured by different routes, such as forging and casting is not available. A consistent view on the characteristics and inter-relationships of thermal fatigue and rolling contact fatigue is also not available.

In view of the above, an exercise was undertaken to assess the fatigue and fracture behaviour of cast and forged railway wheels. In the investigation, the resistance to 'long' fatigue crack growth and the fracture toughness of cast and forged rail wheel materials were evaluated. These properties can be said to control the occurrence of the events at (iii) and (iv) in the sequence outlined above. Since both manufacturing processes are known to produce directionally oriented anisotropic microstructures, the properties were evaluated for radial and circumferential crack extension in the web and in the rim regions of the wheels. Additionally, the behaviour of the material for transverse crack growth in the rim was also studied.

EXPERIMENTAL

Material and specimen fabrication

The railway wheels used in this investigation were commercially produced cast wheels and forged wheels that are used in the railway industry. Wheel quarters for each type were obtained from a wheel manufacturing plant. The chemical compositions of the two wheel materials are given in Table 1.

Table 1 Chemical composition of the cast and forged rail wheel material in wt.%

	C	Mn	Si	S	P	Cr
Cast	0.58	0.663	0.537	0.006	0.05	0.17
Forged	0.56	0.85	0.163	0.006	0.05	0.11

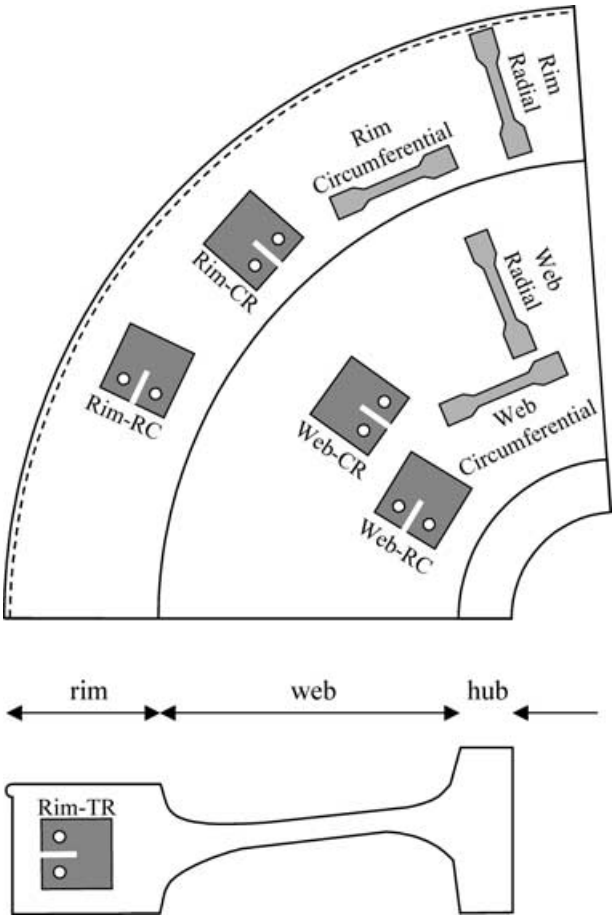

Fig. 1 Schematic of railway wheel showing orientation and nomenclature of specimens.

Round tensile specimens of 5 mm gauge diameter were fabricated in radial and circumferential directions from both the rim and web of the railway wheels. For evaluating fatigue and fracture behaviour of the wheel materials, compact tension (CT) specimens were used. The nominal width of CT specimens used was 50 mm. The nominal thickness was 25 mm for specimens machined from the rim region, and 20 mm for specimens from the web region. Although 25 mm is the standard thickness of 50 mm width CT specimen, this deviation in specimen thickness was required to be made due to the lower net thickness available at the web. Specimens were fabricated by wire-cut electro-discharge machining (EDM) in order to ensure high levels of precision and alignments demanded for fracture mechanics specimens. A cut-up plan giving specimen orientation and nomenclature used in this paper is available in Fig. 1. In the case of CT specimens, the last two letters indicate the orientation of the specimen. For example, in *RC* the first letter indicates the loading direction and the second letter denotes the crack growth direction. The letters *R*, *C* and *T* represents the radial, circumferential and transverse directions of the wheel. A prefix of *Rim* or *Web* has been used additionally with the nomenclature shown in Fig. 1 to indicate the region from where the specimen is fabricated. In this investigation, wherever possible, the nomenclature of specimens is written in expanded form for convenience.

Tensile tests

Tensile tests were carried out as per ASTM standard E 8M.[15] An actuator speed of 0.003 mm/s was used throughout the test. Strain was monitored using a 25 mm gauge length extensometer. The data acquisition rate was kept at 0.25 Hz to provide ~800 points to describe the stress–strain curve. A software developed in-house was used for test control and data acquisition.

Fatigue crack growth rate test

Fatigue crack growth rate (FCGR) tests were conducted using CT specimens as per the methodology laid down in ASTM standard E647.[16] Tests were carried out in digital servohydraulic testing systems under software control. The software had provisions for implementing various ΔK envelopes. FCGR tests were conducted under decreasing ΔK envelopes.* The applied ΔK at any instant was calculated using[16]

$$\Delta K = \Delta K_{\mathrm{o}} \mathrm{e}^{-0.08(\mathrm{a}-\mathrm{a}_{\mathrm{o}})}, \tag{1}$$

where ΔK_{o} and a_{o} refer to the ΔK and crack length with which the test was initiated.

Tests were initiated at relatively higher levels of stress intensity factor range ΔK, which was continuously decreased using Eq. (1). It may be noted that the above procedure for conducting decreasing ΔK FCGR tests was originally proposed by Saxena et al.[17] It is based on the requirement that the monotonic plastic zone associated with $K_{\max}$ of the fatigue cycle should be decreased 'at a rate such that the fractional change in the (plastic) zone size remains constant with increase in *a*' so that there are no delay or retardation effects originating from the progressive unloading. Crack lengths were measured on-line

* ASTM standard E647 (sec. 8.6) specifies that *K*-decreasing tests are not recommended at fatigue crack growth rates above 10^{-5} mm/cycle since prior loading history may affect near threshold crack growth behaviour. In order to rationalise the effect of prior loading history the standard proposes comparison of FCGR data obtained by *K*-decreasing and constant load amplitude procedures to ensure that the crack growth rates (in the region of interest) obtained by the two methods are similar. In this work, tests were conducted on at least two specimens extracted from the rim and web regions (in two orientations) of both types of wheel materials first by the *K*-decreasing method followed by constant load amplitude procedure on the same specimen. The crack growth rates obtained by the two methods were found to be similar. A typical comparison is shown in Fig. 2. It may be noted, nevertheless, that the starting $\mathrm{d}a/\mathrm{d}N$ values were higher (~10^{-4} mm/cycles) than the ASTM recommendations of 10^{-5} mm/cycle.

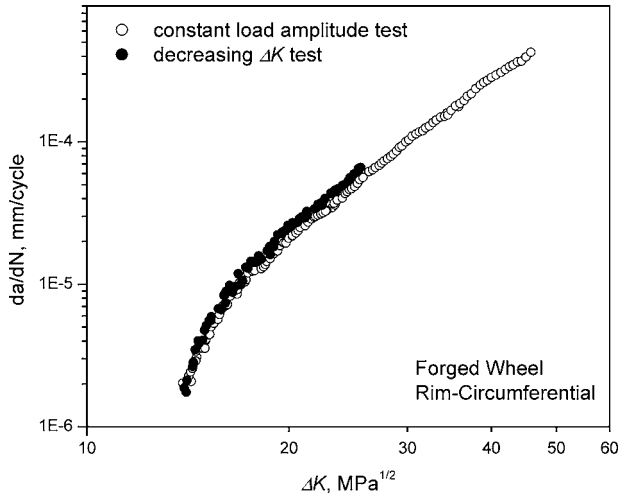

Fig. 2 A typical comparison of FCGR data obtained employing constant load amplitude and decreasing ΔK test procedures.

by a compliance technique using a 5 mm gauge length crack opening displacement (COD) gauge attached to the integrally machined specimen knife edge at the load-line and employing a compliance crack length (CCL) relation suggested by Saxena and Hudak.[18] Crack closure was also monitored on-line following the method recommended in the ASTM E647[16] standard as described below. During every load cycle, more than 200 load-displacement (P, v) points were collected. Open-crack compliance was calculated by considering the data points falling within a window of 50–90% of the maximum load in the cycle. The segmental compliance was calculated from incrementally overlapping segments of 12 points each. The percent deviations of segmental compliance from the open-crack compliance were computed. Starting from maximum of the load cycle, the closure load was identified as the median load of the segment for which the deviation was >2%. FCGRs, da/dN, were computed by the seven point incremental polynomial method, from the crack length a and the corresponding number of cycles N data, on-line. The software for FCGR evaluation saved the relevant data, including ΔK, da/dN, ΔK_{eff} etc. Tests were continued without interruption until the threshold value of ΔK, designated as ΔK_{th}, was reached. Typically this required about 10–15 million cycles. All tests were carried out at a load ratio, R, of 0.1, employing a frequency of 20 Hz at ambient temperature.

Fracture toughness testing

Fracture toughness tests were carried out with CT specimens as per the methodology laid down in ASTM standard E1820.[19] This standard contains the methods for obtaining both the plane strain linear elastic fracture mechanics (LEFM) parameter K_{Ic} and the elastic–plastic fracture mechanics (EPFM) ductile fracture parameter $\mathcal{J}_{\text{Ic}}$. As is apparent later, both the techniques had to be used in this investigation due to the difference in the fracture response of the cast and forged materials. It may be pointed out that the E1820 standard includes the methods contained in the well-known ASTM standard E399[20] for determination of K_{Ic}, and also those contained in the ductile fracture toughness test standards E813[21] and E1737,[22] both of which have now been withdrawn by ASTM.

Prior to carrying out fracture toughness tests, CT specimens were pre-cracked up to a/W ratios of 0.45 to 0.55 (a being the crack length and W the specimen width) following the method described earlier. For determination of LEFM fracture toughness, K_{Ic}, specimens were ramp-loaded until fracture instability, often accompanied by a 'pop-in', was manifested. The load-line displacement was measured using a 5 mm gauge length COD gauge attached to the integral knife-edges on line joining the hole centres of the CT specimen. The load and load-line displacement data collected during the test was used to calculate the fracture toughness. For determination of EPFM fracture toughness, $\mathcal{J}_{\text{Ic}}$, necessitated for cases where the toughness is of a higher level, the single specimen test procedure was adopted. In this, a number of periodic partial unloading was implemented while a specimen was ramp-loaded. The load–unload sequences are repeated *ad infinitum* until substantial amount of crack extension through ductile tearing has taken place. Load-line displacements were measured as in the case of K_{Ic} testing. From the compliance exhibited by the specimen at each unloading step, the instantaneous crack length in the specimen was calculated using the CCL relation alluded to earlier. The $\mathcal{J}$-integral at each of these unloading instances was calculated from the envelope load–load-line displacement curve in an incremental fashion, and, when coupled with the crack extension data, provided the $\mathcal{J}$–resistance (or $\mathcal{J}$–R) curve. The critical $\mathcal{J}$-integral at which ductile crack extension initiated was designated as the ductile fracture toughness of the material. Tests were conducted in a servohydraulic test machine and a software was used for total test control and data acquisition. All fracture toughness tests were carried out under displacement control at a constant displacement rate of 0.003 mm/s.

The procedure for evaluation of LEFM fracture toughness is quite straightforward, being possible to be implemented graphically. On the other hand, for EPFM fracture toughness, data analysis is involved, requiring extensive computations. An in-house developed software was employed for EPFM fracture toughness determination from digitally acquired test data. This software, after constructing the $\mathcal{J}$–resistance curve, adopts the iterative procedure suggested in the ASTM standard E1820[19] to get the blunting line slope and the coefficients of the power law, $\mathcal{J} = C_1 \Delta a^{C_2}$.

RESULTS AND DISCUSSION

Tensile behaviour

The results obtained from the tensile tests conducted on railway wheel materials are summarised in Table 2. The results shown are the average of three tests and the variation in tensile properties were noted to be below ±6%. Typical stress–strain curves obtained from the tensile tests are shown in Figs 3 and 4 for cast and forged wheel materials, respectively. In each figure, plots for radial and circumferential orientation of specimen from both the rim and web region of the wheels are shown.

It can be seen from Table 2 that in both cast and forged wheels, the yield strength (σ_{YS}) and ultimate tensile strength (UTS) were higher in the rim region as compared to the web region. It is also apparent that in general the cast material shows higher strength properties and concomitantly lower ductility properties in comparison to the forged material. This is significant from the viewpoint that fracture toughness is liable to be lower for materials with higher strengths and low ductility. Hence, it may be expected that the forged wheel material will exhibit superior fracture toughness in comparison to the cast wheel material, unless other overwhelming microstructural factors, originating from the difference in the processing routes of the two types of wheels, are operative.

Table 2 Tensile properties of cast and forged railway wheels

Wheel/Region-Orientation	σ_{YS} (MPa)	UTS (MPa)	% El.	% R.A.
Cast				
Rim-circumferential	517	935	11.3	16.2
Rim-radial	486	809	9.3	9.1
Web-circumferential	420	806	10.3	16.1
Web-radial	413	784	10.8	10.9
Forged				
Rim-circumferential	536	900	18.7	39.4
Rim-radial	507	857	14.8	19.5
Web-circumferential	368	747	19.8	42.8
Web-radial	383	757	23.4	39.5

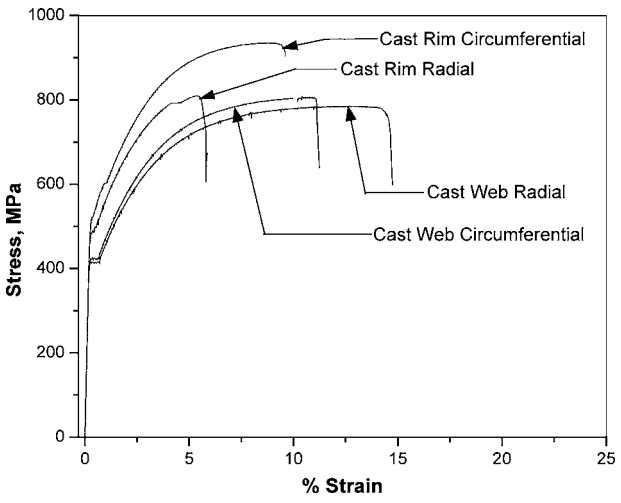

Fig. 3 Tensile stress–strain plots for cast wheel material.

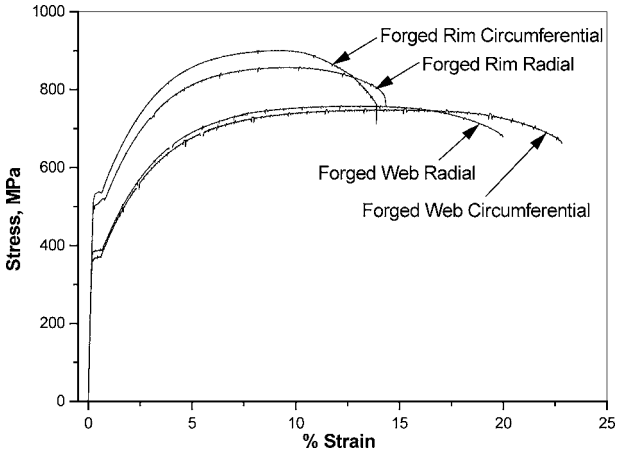

Fig. 4 Tensile stress–strain plots for forged wheel material.

FCGR behaviour

At least three FCGR tests were carried out for each specimen configuration from each of the two types of wheels. The crack growth resistance obtained from replicate tests matched well (e.g., Fig. 5), indicating the uniformity of material property for a given crack plane orientation. The repeatability of test results, particularly at low levels of

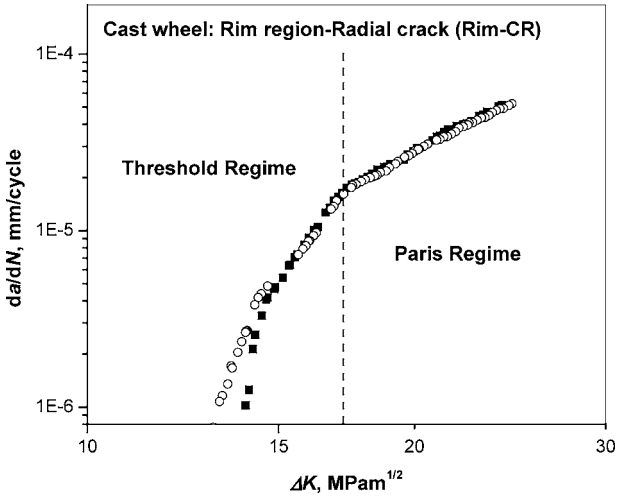

Fig. 5 FCGR plots of replicate tests obtained from Rim-CR specimens of cast wheel.

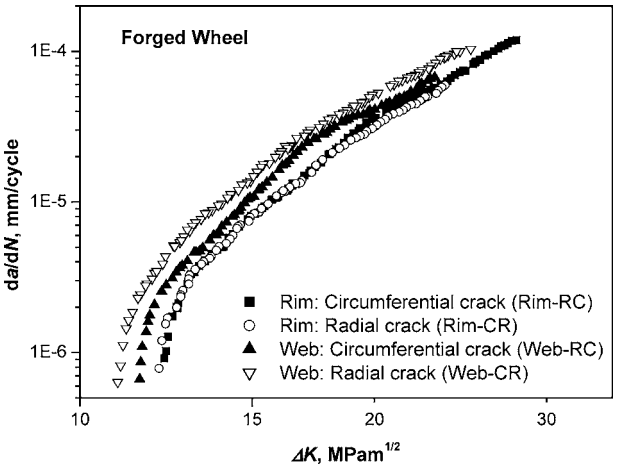

Fig. 6 FCGR plots of the forged railway wheel material for the various orientations and locations of specimens.

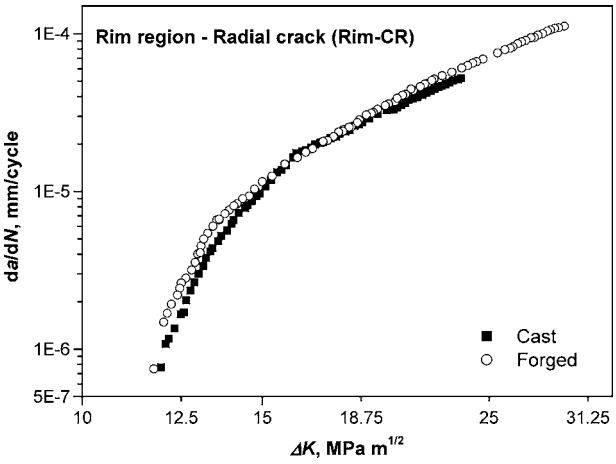

Fig. 7 FCGR curves for cast and forged wheels obtained from specimens fabricated from the rim region, with radial crack orientation.

ΔK, also upholds the robustness of the computer controlled testing procedure employed. Figure 5 shows the FCGR plots obtained from two specimens fabricated from the rim region of cast wheels with radial crack plane orientation. It can be noted that the Paris regime FCGR data from replicate tests superimpose well, and only a nominal (± 1 MPa$\sqrt{\text{m}}$) difference was noted in the ΔK_{th} values from the two tests. Similar coincidence of FCGR plots is observed for replicate tests in other specimen orientations in both types of wheels.

The fatigue crack growth resistances of railway wheel material in various orientations of crack growth were found to be similar. Figure 6 presents FCGR plots of forged wheel specimens machined in both the orientations from the rim as well as the web region. It can be seen that the FCGR plots of various types of specimens fall within a narrow band. On closer inspection, it appears that the fatigue crack growth resistance of the web region is somewhat inferior to that of the rim region. The web region showed an apparent higher crack growth rate (and lower ΔK_{th}) in comparison to the rim region in both orientations. However, if the magnitude of the difference and the scatter normally associated with FCGR data (a fraction, typically one-fifth of an order of magnitude) is considered, this difference may not be significant.

A typical comparison of the behaviour of cast and forged microstructures from equivalent wheel region and equivalent crack growth plane is shown in Fig. 7. It is apparent from the plots in Fig. 7 that the fatigue crack growth resistances of the cast and forged material are similar through a large range of crack driving force ΔK. Similar behaviour was observed in other cases also.

From FCGR plots of various specimen orientations in the two types of railway wheel, ΔK_{th}, C and m were determined. Here, ΔK_{th} is the threshold value of ΔK, C and m are the intercept and slope of the linear region of the FCGR data obeying the Paris equation $\text{d}a/\text{d}N = C\Delta K^{\text{m}}$. As per the ASTM standard, ΔK_{th} should be determined at the crack growth rate of 10^{-7} mm/cycle by linear best-fit method for a minimum of five data points between the crack growth rates of 10^{-6} and 10^{-7} mm/cycle. However, as in this investigation sufficient lower $\text{d}a/\text{d}N$ data (say below 10^{-6} mm/cycle) was not generated, a linear best-fit line was constructed to the five lowest decade of data available and was extrapolated to the crack growth rate of 10^{-7} mm/cycle. This extrapolated value of ΔK corresponding to the crack growth rate of 10^{-7} mm/cycle is considered as ΔK_{th}. It must be mentioned that the intension of ΔK_{th} here is not to define a true threshold value of ΔK, but rather to provide a mere comparison of the near threshold fatigue crack growth behaviour of the two steels. For obtaining the C and m values, a best-fit line was drawn to the linear region of data points obeying the Paris equation such that the correlation coefficient is at least 0.99. The average values of the characteristic parameters obtained from multiple tests are listed in Table 3. The actual range of data points used for determining the Paris constants is included in this table. From a comparison of the characteristic parameters, it can be said that the resistance to fatigue crack growth of the cast and forged materials are very similar for equivalent orientation and location of the crack plane. It can also be seen from Table 3 that the Paris slope m is consistently higher for circumferential crack growth in the rim and radial crack growth in the web for both the cast and the forged material. Table 3 reveals that ΔK_{th} is largely similar, and of considerably high value for tests conducted at $R = 0.1$, at all orientations of crack growth in both regions of the two types of wheel. The latter is indicative of the fact that both wheels exhibit crack closure that effectively decreases the driving force

Table 3 FCGR characterizing parameters of cast and forged railway wheels

Wheel/Region-orientation	C note 1	m note 1	ΔK_{th} note 2	ΔK range used for obtaining C and m
Cast				
Rim-Circumferential	1.080×10^{-10}	4.073	12.65	24–15
Rim-radial	1.079×10^{-9}	3.345	12.97	23–16
Rim-transverse	6.344×10^{-10}	3.539	12.30	23–15
Web-circumferential	7.056×10^{-10}	3.591	11.90	29–16
Web-radial	3.327×10^{-11}	4.606	12.54	27–18
Forged				
Rim-circumferential	7.387×10^{-11}	4.301	12.18	27–17
Rim-radial	8.209×10^{-10}	3.525	12.07	23–16
Rim-transverse	5.050×10^{-10}	3.682	12.01	23–16
Web-circumferential	7.939×10^{-10}	3.614	11.04	23–16
Web-radial	3.608×10^{-10}	3.924	11.33	24–15

note 1: C and m are calculated for da/dN in mm/cycle and ΔK in MPa$\sqrt{}$m
note 2: Units of ΔK_{th} is MPa$\sqrt{}$m

responsible for crack growth. The effect of crack closure is manifested most perceptibly in the threshold regime, where the crack driving force is low and therefore more liable to be suppressed through crack closure. In the present case, it was established that the effective ΔK_{th} levels (i.e. when the crack closure contributions were removed by numerical reduction of closure) were in the range of 4–6 MPa$\sqrt{}$m.

As mentioned earlier, crack closure was monitored online during FCGR tests in this investigation. From the closure measurements, the effective ΔK available to the crack tip, ΔK_{eff}, was calculated. It was observed that ΔK_{eff} was a fraction of the ΔK that is applied (ΔK_{app}) which diminished with decreasing values of ΔK. The behaviour shown in the cases of circumferential crack specimens extracted from the rim region of cast and forged wheels are shown in Figs 8 and 9 as examples. It is obvious from the figures that the reduction in the applied ΔK due to crack closure is higher at lower values of ΔK.

FCGR plots characterised by ΔK_{eff} (Figs 8 and 9) can be used to represent the intrinsic resistance of the materials to fatigue crack extension. The intrinsic fatigue crack growth resistance of the cast material for most of the specimen configurations tested is shown in Fig. 10. A similar situation as in Fig. 6 is manifested—all the FCGR plots falling within a narrow band. Figure 10 indicates that some of the scatter (as in Fig. 6) is due to variations of operative crack closure.

It is instructive to compare the intrinsic fatigue crack growth resistance of the cast and forged wheel material. Figures 11 and 12 show the comparative resistance of the two materials for rim-radial and web-circumferential

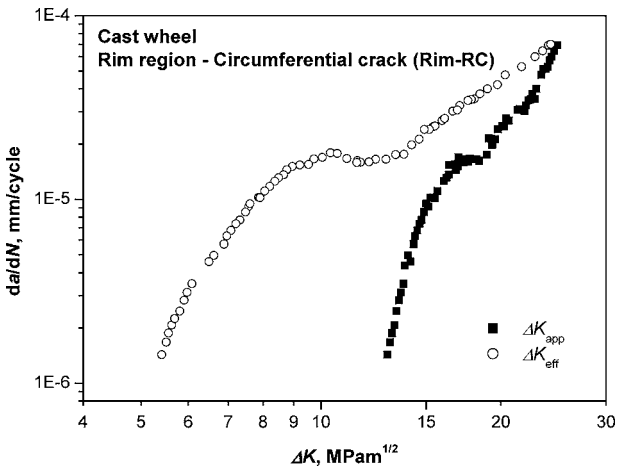

Fig. 8 Fatigue crack growth resistance of cast material from rim region with circumferential crack characterised by applied and effective ΔK.

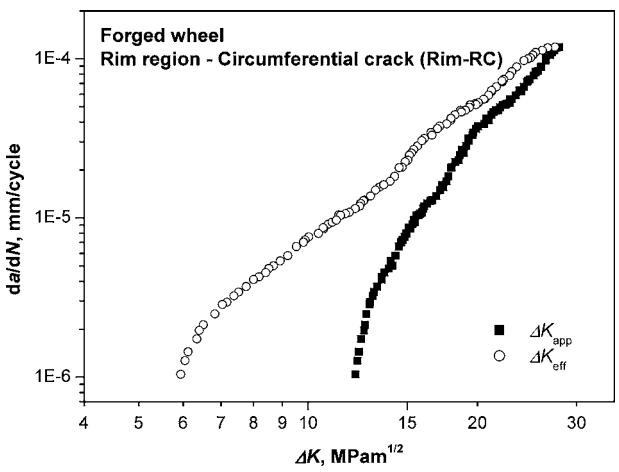

Fig. 9 Fatigue crack growth resistance of forged material from rim region with circumferential crack characterised by applied and effective ΔK.

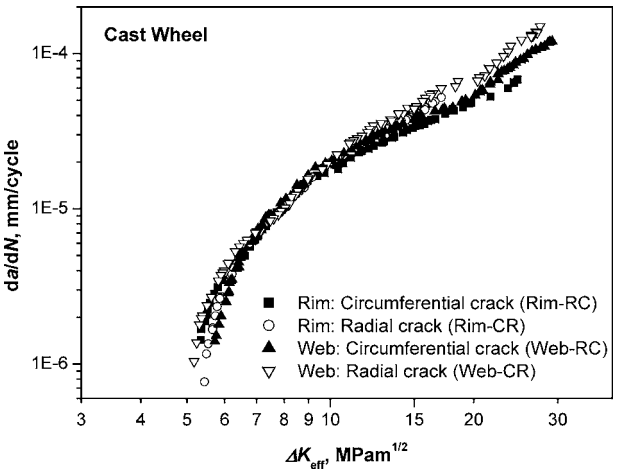

Fig. 10 FCGR plots, characterised with ΔK_{eff}, of the cast railway wheel material for the various orientations and locations of specimens.

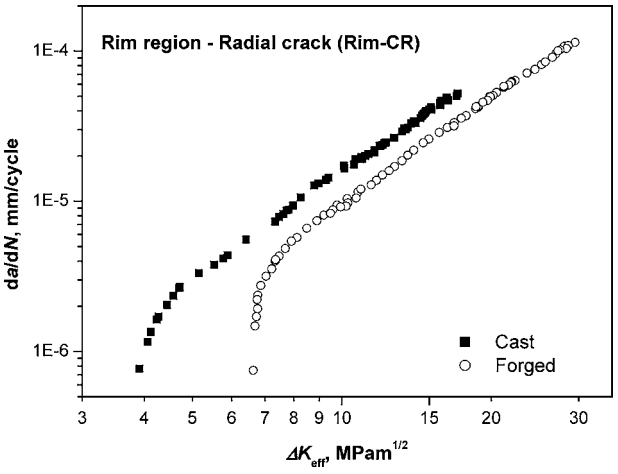

Fig. 11 Comparison of intrinsic fatigue crack growth resistance of the cast and forged material from the rim region of wheels for radial crack extension.

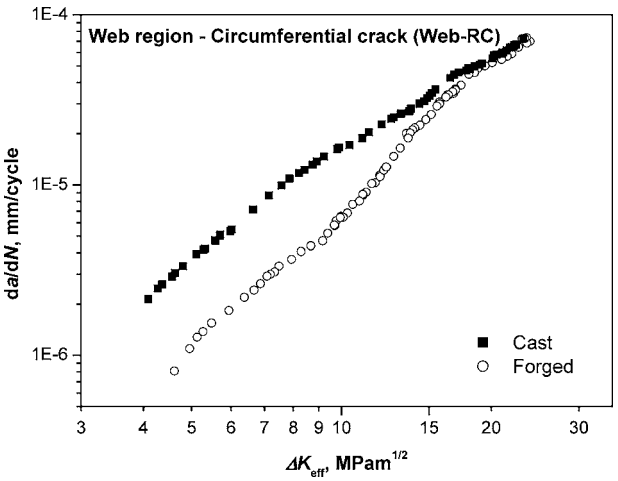

Fig. 12 Comparison of intrinsic fatigue crack growth resistance of the cast and forged material from the web region of wheels for circumferential crack extension.

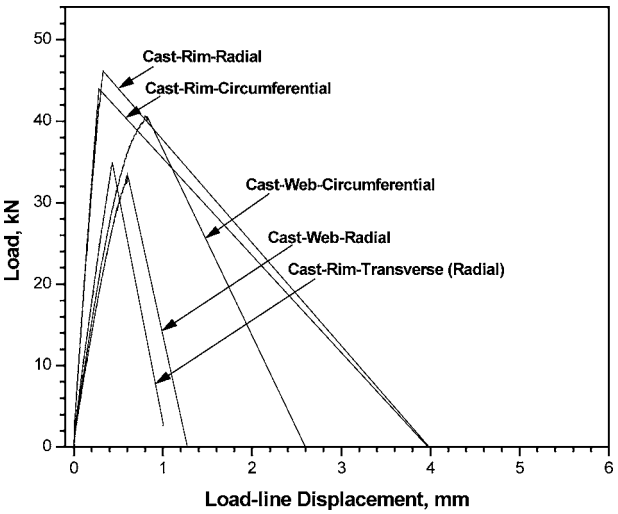

Fig. 13 Load–displacement plots from fracture toughness tests on specimens fabricated from cast rail wheel.

specimen configurations, respectively. It can be seen from both the figures that the forged material is intrinsically superior to the cast material due to the lower FCGR exhibited by it at any given value of actual crack driving force ΔK_{eff}. With this hindsight, it can be said that the cast material compared equivalently with the forged material when characterised by applied ΔK (see Fig. 7) only because of the enhanced levels of crack closure manifested in it.

Fracture toughness

Although there is similarity between the tensile properties and the fatigue crack growth resistance of cast and forged railway wheels (notwithstanding the differences in ductility and intrinsic fatigue crack growth resistance of the materials), the fracture characteristics of the two types of materials were found to be entirely different. This dissimilarity is best portrayed by the nature of the load–displacement plots obtained during fracture toughness testing in the two cases. Figures 13 and 14 show such plots for specimens extracted from the cast and forged wheels, respectively. It can be seen that the cast material (Fig. 13) exhibits catastrophic fracture without substantial deviation from elastic deformation behaviour for all locations and orientations of specimens. Materials such as these are amenable to treatment through LEFM formulation, and it is likely that it may be possible to characterize their fracture behaviour by the LEFM fracture

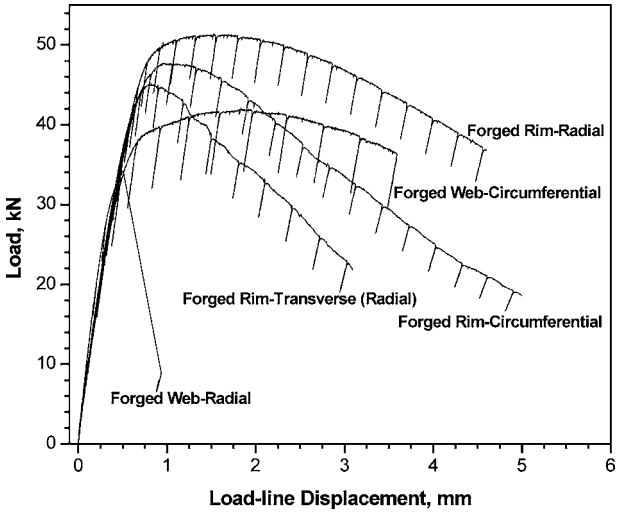

Fig. 14 Load–displacement plots from fracture toughness tests on specimens fabricated from forged rail wheel.

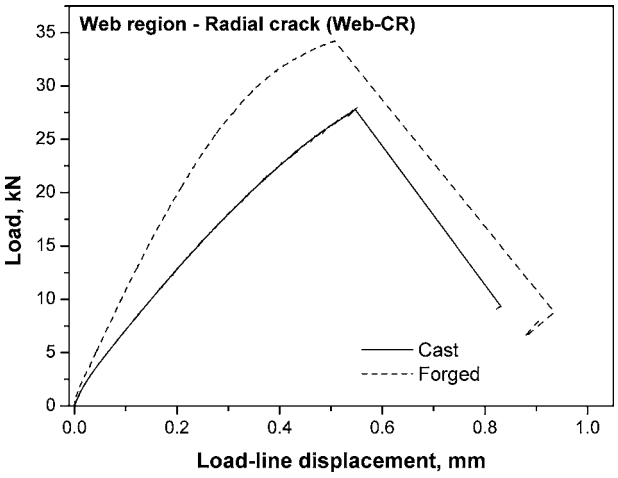

Fig. 15 Load–displacement plots obtained during fracture toughness tests conducted on specimens from the web region of cast and forged wheels with radial crack orientation.

toughness parameter K_{Ic}. The forged material, on the other hand, shows (Fig. 14) considerable plastic deformation and the load–displacement plots exhibit substantial deviation from the elastic loading line as it is stressed. Fracture in these cases is through stable extension of cracks, unlike the catastrophic instability in the cast material. The fracture behaviour can be said to be falling under the category of EPFM and the fracture toughness, in this case, can be characterized by $\mathcal{J}_{Ic}$ obtained from the $\mathcal{J}$–R curve. In spite of the apparent applicability of LEFM or EPFM, the validity of the respective parameters (K_{Ic} or $\mathcal{J}_{Ic}$) has to be ensured through the fulfilment of certain criteria, as discussed later.

It may be noted in Fig. 14 that the plot for web-radial specimen of forged wheel exhibits catastrophic behaviour, similar to that observed in cast wheel specimens. The behaviour of web-radial specimens for both cast and forged wheel materials are compared in Fig. 15 to bring out the similarity. The fracture behaviour of the forged material for the web-radial specimens is thus different from that of the other specimens.

For LEFM-type fracture behaviour, a critical load P_Q can be identified, as per the method of ASTM standards E399[20] or E1820,[19] and a tentative fracture toughness K_Q can be calculated from it. For this, the pre-fatigue crack length a_o has to be accurately determined post-test by averaging a number of measurements made along the crack-front. K_Q will be qualified as K_{Ic} if the following dimensional and load criteria are satisfied

$$(W - a_o) \quad \text{and} \quad B \geq 2.5\left(\frac{K_Q}{\sigma_{YS}}\right)^2, \tag{2}$$

$$\frac{P_{max}}{P_Q} \leq 1.1. \tag{3}$$

In the above equations W is the specimen width, B is the specimen thickness, σ_{YS} is the yield stress of the material and P_{max} is the maximum load of the load–displacement plot.

In spite of the apparent incompatibility (in terms of the shape of the load–displacement curve) of the forged material for LEFM characterization, K_Q was evaluated for all of the variety of specimens, for both the cast and forged wheel materials. The average values obtained from multiple specimens are reported in Table 4. The minimum B necessary in order to qualify the K_Q as K_{Ic} as per Eq. (2) and the experimental P_{max}/P_Q obtained are included in this table along with the actual specimen thickness (B) and the uncracked ligament (W-a_o) dimension. It can be seen from Table 4 that none of the specimen orientations in both the cast and forged materials are able to satisfy both the criteria in Eqs. (2) and (3). Since P_{max}/P_Q is >1.1 for a majority of cases, the strength ratios (R_{SC}) of the specimens were compared, as suggested in ASTM E 399. This will provide a comparison of the load-bearing capacity of similar-sized specimens and is a function of the maximum load that the specimen can sustain, its initial dimensions and yield stress. Strength ratios for CT specimens were computed using the following relation

$$R_{SC} = \frac{2P_{max}(2W + a)}{B(W - a)^2\sigma_{YS}}, \tag{4}$$

where P_{max} is the maximum load, B is the specimen thickness, W is the specimen width, a is the crack length and σ_{YS} is the yield stress of the material. The calculated R_{SC} values are included in Table 4. The specimen strength ratios of cast specimens were slightly inferior to that of the forged specimens. As none of the specimens satisfied both the qualifying criteria given in Eqs. (2) and (3), LEFM cannot be used to characterize the fracture toughness in

Table 4 Unqualified fracture toughness of cast and forged railway wheels. The minimum thickness requirements, experimental P_{max}/P_Q observed and the specimen strength ratio (R_{SC}) are given. Table also shows the actual dimensions of the specimens tested

Wheel/Region-orientation	K_Q (MPa$\sqrt{m}$)	$2.5\left(\frac{K_Q}{\sigma_{YS}}\right)^2$ (mm)	$\frac{P_{max}}{P_Q}$	R_{SC}	actual B (mm)	actual (W-a_o) (mm)
Cast						
Rim-circumferential	71.16	46.46	1.00	1.496	24.86	24.71
Rim-radial	71.65	54.94	1.00	1.478	24.87	24.61
Rim-transverse	69.79	45.74	1.01	1.447	24.93	23.27
Web-circumferential	69.08	67.65	1.26	2.039	19.90	24.85
Web-radial	67.99	68.32	1.21	1.858	19.90	23.22
Forged						
Rim-circumferential	79.13	54.78	1.24	1.859	24.96	22.68
Rim-radial	89.71	78.34	1.11	1.868	24.90	22.90
Rim-transverse	80.16	55.98	1.15	1.685	24.96	24.20
Web-circumferential	75.60	105.51	1.15	2.086	19.92	24.23
Web-radial	69.19	81.61	1.19	2.150	19.94	22.77

the two types of wheels. It should be noted that it would not have been physically possible to fabricate fracture mechanics specimens of qualifying dimensions from the geometry of the railway wheels. The contour of the web particularly does not allow more than ~20 mm thickness in case of the cast wheels.

Since LEFM based fracture toughness could not be validated for both the cast and the forged wheel material, attempt was made to obtain EPFM based characteristic fracture toughness values given in terms of the $\mathcal{J}$-integral. All of the forged wheel specimens, except those extracted from the web region with radial orientation of crack, yielded $\mathcal{J}$–R curves from which the critical resistance to fracture, $\mathcal{J}_Q$, could be obtained. For the specimens obtained from the cast wheel, and the forged web-radial specimens, in which unstable crack propagation ensued prior to the onset of ductile crack extension, $\mathcal{J}$–R curves or $\mathcal{J}_Q$ values could not be elicited. $\mathcal{J}_{Qc}$ values were calculated for these cases as per the basic method for determination of fracture instability toughness given in Appendix 6 of ASTM standard E-1820.[19]

Typical $\mathcal{J}$–R curves for the forged material are given in Fig. 16. It may be pointed out that a higher $\mathcal{J}$–R curve signifies an improved resistance of the material to fracture. In Fig. 17, the identification of $\mathcal{J}_Q$ on a $\mathcal{J}$–R curve, as per the methods of ASTM standard E-1820,[19] for a particular case of forged-rim specimen with circumferential crack orientation is shown. To qualify $\mathcal{J}_Q$ as the ductile fracture toughness $\mathcal{J}_{Ic}$, the criteria

$$(W - a_o) \quad \text{and} \quad B \geq 25\frac{\mathcal{J}_Q}{\sigma_Y}, \tag{5}$$

$$\left.\frac{d\mathcal{J}}{da}\right|_{\Delta a_Q} < \sigma_Y \tag{6}$$

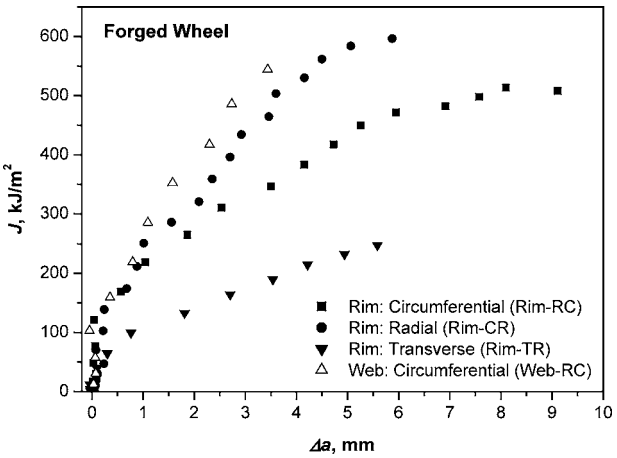

Fig. 16 $\mathcal{J}$–R curves obtained from specimens of the forged rail wheel.

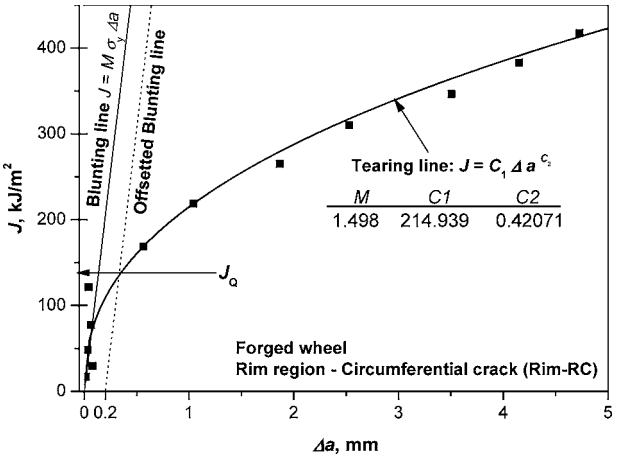

Fig. 17 Identification of $\mathcal{J}_Q$ on the $\mathcal{J}$–R curve obtained from a rim-circumferential specimen of the forged rail wheel.

have to be satisfied. In the above equation σ_Y is the flow stress, given as the mean of the yield stress and the ultimate strength, and Δa_Q is the crack extension at $\mathcal{J}_Q$.

$\mathcal{J}_{Qc}$ is calculated by the basic method of $\mathcal{J}$-integral calculation by summation of the elastic $\mathcal{J}$, obtained from the stress intensity factor K for the identified critical load at which fracture instability occurs, and the plastic $\mathcal{J}$, obtained from the plastic area under the load–displacement plot up to the critical load. $\mathcal{J}_{Qc}$ is qualified as $\mathcal{J}_c$, the fracture instability toughness, if a size criterion similar to that in Eq. (5) with the constant 25 replaced by 100 (for the class of steel like the rail wheel materials) is met, and provided that more than 0.2 mm actual ductile crack extension has not occurred prior to the onset of fracture instability. Reference may be made to ASTM standard E 1820[19] for a detailed understanding of the nomenclature and definitions of the various critical parameters.

It was found that all of the values of $\mathcal{J}_Q$ and $\mathcal{J}_{Qc}$ obtained for the specimens with various crack plane orientations from the rim as well as the web regions of cast and forged rail wheels qualified to be termed as $\mathcal{J}_{Ic}$ and $\mathcal{J}_c$, respectively. This means that the fracture toughness values are size and geometry independent, and therefore amenable to comparisons. The average values obtained for the various types of specimens are listed in Table 5. Included in Table 5 are the minimum requirements of thickness and remaining ligament (W-a_o) for valid fracture toughness measurement, obtained from the size criterion given earlier. Footnotes at the bottom of the table clarify which of the fracture toughness values are obtained as $\mathcal{J}_{Ic}$ and which as $\mathcal{J}_c$.

From Table 5, it can be said unequivocally that the material of cast rail wheels has, in general, lower fracture toughness than that of forged rail wheels. It appears that the material of the web of cast wheels has a superior resistance to fracture than that of the rim region. In the forged rail wheel, the rim material is equal, if not better, than the web region in terms of fracture resistance. For radial cracks growing in the web region, and transverse cracks in the rim region, the fracture toughness seems to be the lowest in forged wheels. However, even here the toughness is above that of the cast wheel material.

Table 5 Qualified fracture toughness of cast and forged railway wheels. The minimum thickness requirements are given

Wheel/Region-orientation	$\mathcal{J}_{Ic}$ or $\mathcal{J}_c$ (kJ/m^2)	$25\left(\frac{\mathcal{J}}{\sigma_Y}\right)$ (mm)
Cast		
Rim-circumferential	25.52#	2.87
Rim-radial	27.55#	2.80
Rim-transverse	27.44#	3.08
Web-circumferential	62.42#	7.75
Web-radial	44.57#	5.42
Forged		
Rim-circumferential	140.74*	4.73
Rim-radial	143.05*	4.98
Rim-transverse	61.09*	2.24
Web-circumferential	145.33*	6.37
Web-radial	75.94#	10.24

*obtained as $\mathcal{J}_{Ic}$ # obtained as $\mathcal{J}_c$

The inferior fracture behaviour of cast wheel material is further investigated through careful examination of the fracture surface. Figure 18 shows the typical fracture surfaces that are produced in the rim and web CT specimens of the cast wheel for both circumferential and radial crack extension. The brittle nature of the fracture surfaces is immediately evident. It can be seen that for rim specimens fracture is associated with chevron marks that can be traced back to the point of origin of catastrophic fracture, whereas in both circumferential and radial specimens from the web, a small amount of ductile crack extension has taken place. The relative ductile fracture behaviour of the web region is primarily due to the lower thickness of the web specimens, and hence the greater plastic deformation that they can manifest. This ductile nature originating from ductile tearing is the reason for the nonlinearity in the P–v curve in Fig. 13 and the high value of P_{max}/P_Q (Table 4). Employing a plastic zone size correction to the crack length, the nonlinearity may be partly accounted for through a change in compliance as the plastic zone develops with increase in load.[23]

The brittle nature of the fracture surface of the cast material with predominant chevron markings indicates the availability of extraneous inclusions and second phase particles near the crack tip, facilitating unstable crack extension. This was supplemented by the comparison of microstructures of the forged and cast wheel materials as shown in Fig. 19. It can be seen from Fig. 19 that both forged and cast wheel materials posses ferrite-pearlitic structures. However, the cast wheel revealed the presence of a large amount of inclusions in the pro-eutectoid ferritic regions as shown in Fig. 19. Presence of such inclusions can adversely affect the fracture resistance of the material.[24,25] The microstructure of the forged wheel, on the other hand, was observed to be clean (Fig. 19). The poor fracture resistance of the cast wheel in comparison to the forged wheel can therefore be attributed to the inferior material quality.

This investigation brings out the fact that in spite of the advancement in steel- casting technology, producing clean steel for critical application still remains a challenge. Use of inferior quality cast wheels, as observed in this investigation, can lead to catastrophic failure on service/accidental loads. Although the initiation and early growth of fatigue cracks has not been included within the scope of this study, it is expected that the presence of inclusions will

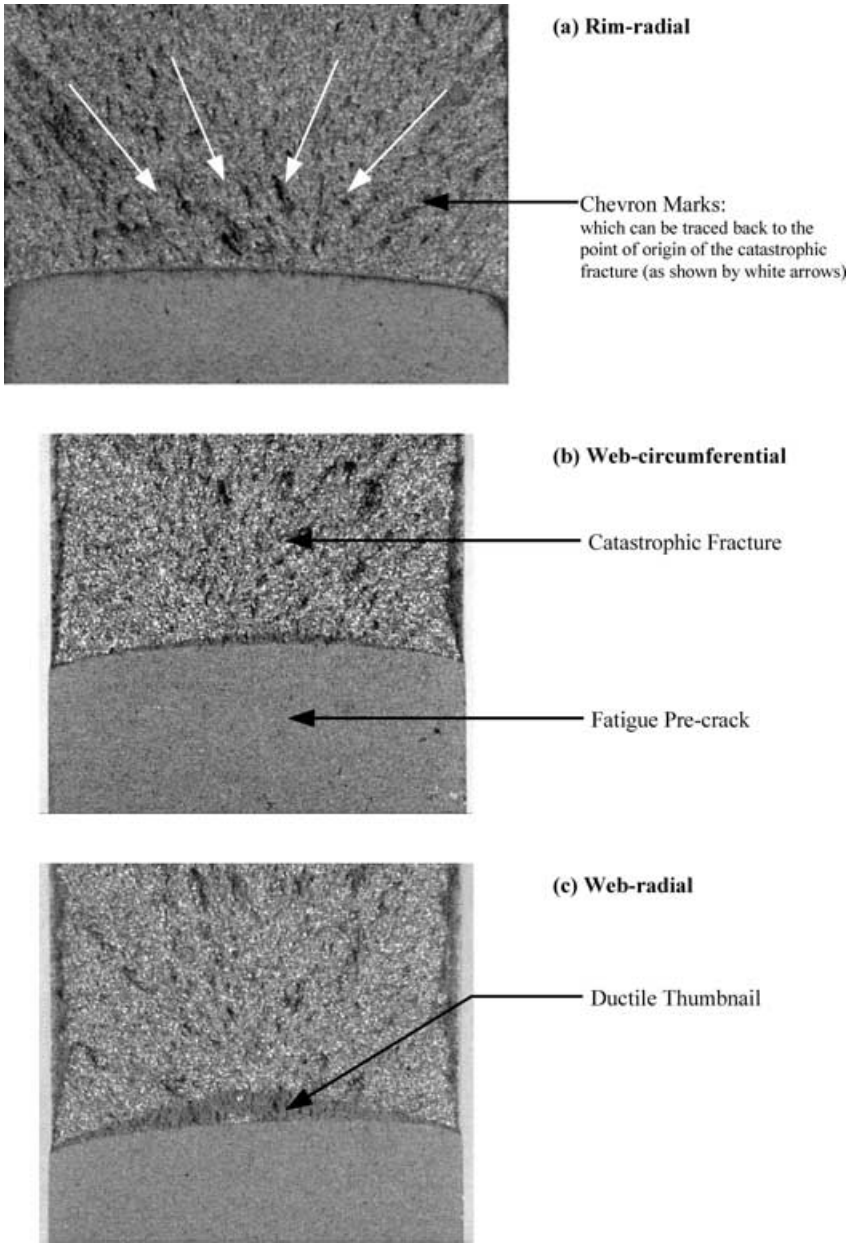

Fig. 18 Details of fracture surfaces from (a) rim-radial, (b) web-circumferential and (c) web-radial specimens of cast wheel material. Annotations identify typical features.

severely compromise the performance of components on these counts also. Substitution of forged wheels by cast wheels for passenger traffic has therefore to be dealt with cautiously.

CONCLUSIONS

From the comparison of the fatigue and fracture behaviour of cast and forged railway wheels, the following generalized conclusions could be arrived at:

1 The material of the cast wheel shows higher strength properties and lower ductility properties in comparison to the material of the forged wheel (in spite of the apparent anomaly for rim-radial direction). In both types of wheels, the strength properties were higher in the rim region in comparison to the web region.
2 The fatigue crack growth resistances of the cast and forged material appear to be similar for equivalent orientation and location. FCGR data from the various regions and orientations fall within a narrow band. For both the cast and the forged rail wheel, the Paris slope (m) is higher for

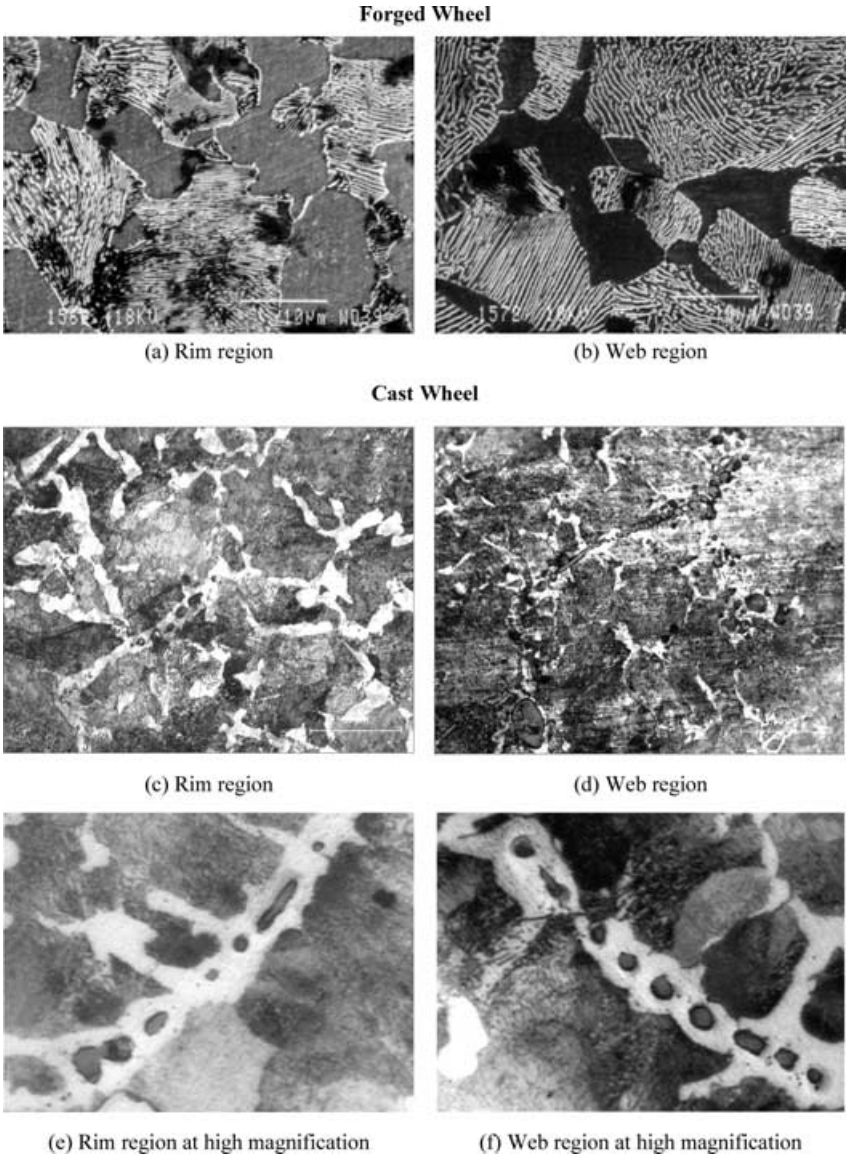

Fig. 19 Microstructure of (a–b) forged rail wheel, (c–d) cast wheel in Rim and Web regions. A close-up picture (×400) of inclusion network in cast wheel is given in (e–f).

circumferential crack growth in the rim and radial crack growth in the web.

3 Higher levels of crack closure were exhibited in the cast material, particularly in the threshold regime. While the apparent resistance to fatigue crack growth appeared to be equivalent in the two materials, the intrinsic resistance to crack extension could therefore be inferred to be inferior in the cast material.

4 The fracture toughness of the cast and forged rail wheel materials could be characterized only by parameters based on the J-integral. LEFM parameters like K_{Ic} could not be qualified to be valid according to ASTM criteria.

5 In general, the forged wheel material exhibited superior fracture toughness in comparison to the cast wheel material. Resistance to fracture was lowest for radial crack growth in the web of forged wheels; however, even this was better than the highest fracture toughness displayed in the cast material.

REFERENCES

1 Polyakov, V. F., Klevakin, V. V., Minevich, V. Ya. and Kosenko, P. Yu. (1990) Production of railway wheels from individual cast semis. *Steel in USSR* **20**, 441–443.

2 Qian, L. and Meng, J. (2000) Study on microstructure of cast wheels. *Iron and Steel (China)* **35**, 45–45.

3 Ekberg, A., Kabo, E. and Andersson, H. (2002) An engineering model for prediction of rolling contact fatigue of railway wheels. *Fat. Fract. Eng. Mater. Struct.* **25**, 899–909.

4 Ekberg, A. and Marais, J. (2000) Effects of imperfections on fatigue initiation in railway wheels. Proceedings of the Institution of Mechanical Engineers, Part F: *J Rail Rapid Transit* **214**, 45–54.
5 *Comparative Assessment of Fatigue and Fracture Behaviour of Cast and Forged Railway Wheels* (2001) Final Project Report No. T/0008/2001, National Metallurgical Laboratory, Jamshedpur.
6 Cabral, A., Thompson, A. W., Bernstein, I. M. and Stone, D. H. (1987) The thermal fatigue behavior of near-eutectoid steel. *Mater. Sci. Eng.* **93**(1–2), 73–82.
7 Sehitoglu, H. (1987) Crack-growth studies under selected temperature – strain histories. *Eng. Fract. Mech.* **26**, 475–489.
8 Fec, M. C. and Sehitoglu, H. (1985) Thermal – mechanical damage in railroad wheels due to hot spotting. *Wear* **102**(1–2), 31–42.
9 Pistorius, P. G. H. and Marais, J. J. (1995) Thermal fatigue of steel tyres on urban railway systems. *Int. J. Fatigue* **17**, 471–475.
10 D'Antonio, C. (1993) Fracture of a train wheel due to thermally induced fatigue and residual stress. *Handbook of Case Histories in Failure Analysis* **2**, 71–72. ASM International, Materials Park, Ohio, USA.
11 Proidak, Yu. S., Gasik, M. I., Kadinov, E. I., Antipov, B. F., Staroseletskii, M. I. and Miroshnichenko, N. G. (1994) Improvement of wheel steel quality during alloying with nitrided FeV in ladle. *Stal'* **7**, 29–30.
12 Bowles, C. Q. and Roland, J. R. (1992) Comparison of the fracture behavior of conventional class U railway wheels and an experimental alloy wheel. *ASTM Jr. Testing and Evaluation* **20**, 408–415.
13 Uwe, Z., Kartin, M. and Hartmut, H. (2005) Fracture mechanics in railway applications—an overview. *Eng. Fract. Mech.* **72**, 163–194.
14 Kuna, M., Springmann, M., Mädler, K., Hübner, P. and Pusch, G. (2005) Fracture mechanics based design of a railway wheel made of austempered ductile iron. *Eng. Fract. Mech.* **72**, 241–253.
15 *ASTM standard E 8M-04* (2005) Test Methods for Tension Testing of Metallic Materials [Metric], Annual Book of ASTM Standards, **03.01**, American Society of Testing and Materials, PA.
16 *ASTM standard E 647–00* (2005) Standard Test Method for Measurement of Fatigue Crack Growth Rates, Annual Book of ASTM Standards, **03.01**, American Society of Testing and Materials, PA, 2000.
17 Saxena, A., Hudak, Jr. S. J., Donald, J. K. and Schmidt, D. W. (1978) Computer controlled decreasing stress intensity technique for low rate fatigue crack growth testing. *Jr. Test. Eval.* **6** 167–174.
18 Saxena, A. and Hudak, Jr., S. J. (1978) Review and extension of compliance information for common crack growth specimens. *Int. Jr. Fracture* **14**, 453–468.
19 *ASTM standard E 1820-99a* (2000) Standard Test Method for Measurement of Fracture Toughness, Annual Book of ASTM Standards, **03.01**, American Society of Testing and Materials, PA, 2000.
20 *ASTM standard E 399-90 (Reapproved 1997)* (2000) Test Method for Plane-Strain Fracture Toughness of Metallic Materials, Annual Book of ASTM Standards, **03.01**, American Society of Testing and Materials, PA, 2000.
21 *ASTM standard E 813-89* (1992) Test Method for J_{Ic}, A Measure of Fracture Toughness, Annual Book of ASTM Standards, **03.01**, American Society of Testing and Materials, PA.
22 *ASTM standard E 1737-96* (1996) Test Method for *J*-integral Characterization of Fracture Toughness, Annual Book of ASTM Standards, **03.01**, American Society of Testing and Materials, PA, 1996.
23 Bucci, J. R., Paris, P. C., Landes, J. D. and Rice, J. R. (1972) *J* integral estimation procedures. Fracture Toughness, Proceedings of the 1971 National Symposium on Fracture Mechanics, Part II, *ASTM STP 514*, American Society for Testing and Materials, 40–69.
24 Sen, S. K., Ray, A., Dhua, S. K., Prasad, M. S., Sabyasachi, S. K., Jha, S., Bhattacharyya, S. K., Choudhury, P. P. and Biswas, U. (1998) Influence of Inclusions and Heat Treatment on Fatigue Strength of Wheel and Axle Steel. *Fatigue Design 1998*. Publ: Technical Research Centre of Finland, Vuorimiehentie, Espoo, Finland, vol. **1**, 309–331.
25 *Failure Analysis of Railroad wheels* (2001) Final Report of Project CIEP (SSP)/2001/0109, National Metallurgical Laboratory, Jamshedpur 831007.

